



IUTAM_ABCM Symposium on Laminar Turbulent Transition
Laminar streaks in oscillating boundary layers

Peter D. Hicks^{a,*}, Pierre Ricco^b

^a*School of Engineering, Fraser Noble Building, King's College, University of Aberdeen, Aberdeen, AB24 3UE, United Kingdom*

^b*Department of Mechanical Engineering, The University of Sheffield, Sheffield, S1 3JD, United Kingdom*

Abstract

The growth of laminar streaks in a flat-plate boundary layer is investigated in the presence of both spanwise wall oscillations and steady streamwise-dependent spanwise wall forcing. The laminar streaks are forced by free-stream vortical disturbances, which interact with the boundary layer to produce disturbances, which first grow and then decay. The oscillating plate produces a base flow that matches Blasius boundary layer in the streamwise and wall-normal directions, but produces a generalized Stokes layer (GSL) in the spanwise direction. This depends on the Blasius flow and tends to the classical Stokes layer (CSL) in the asymptotic limit of high oscillation frequency or large downstream distance. Spanwise oscillations of the plate and spanwise wall forcing can both reduce the total energy and maximum amplitude of the disturbances. Their relative effects are discussed.

© 2015 The Authors. Published by Elsevier B.V. This is an open access article under the CC BY-NC-ND license

(<http://creativecommons.org/licenses/by-nc-nd/4.0/>).

Selection and peer-review under responsibility of ABCM (Brazilian Society of Mechanical Sciences and Engineering)

Keywords: Boundary layer ; Flow control ; Energy reduction

1. Introduction

Laminar streaks (or Klebanoff modes as they are also known), have been observed^{1,2} as a precursor to boundary layer transition in flow near the leading edge of a flat plate, when the level of free-stream turbulence, $Tu \approx 1\%$ or higher. These streaks consist of alternating spanwise regions of high and low streamwise velocity, which can subsequently break down to form turbulent spots and ultimately a fully turbulent flow. Attenuating the growth of laminar streaks is therefore important to delay boundary layer transition, and thus to reduce drag over aircraft aerofoils and turbine blades.

The earliest analysis of laminar streak growth, forced by free-stream vortical disturbances, is due to Leib *et al.*³. This analysis has been extended to consider gas compressibility⁴, the streak structure in the outer portion of the boundary layer⁵ and nonlinear effects⁶. Several approaches to reducing the growth of laminar streaks have been investigated, including wall suction^{7,8,9,10}, wall heating and cooling^{11,12,13}, and steady spanwise wall forcing¹⁴. Spanwise plate oscillations have also been investigated in the context of Görtler vortices above concave surfaces¹⁵. In this paper, within the original linearized incompressible streak framework of Leib *et al.*³, spanwise oscillations above a flat plate are investigated as a streak reduction mechanism and their effectiveness is compared to steady spanwise wall

* Corresponding author. Tel.: +44 1224 274815.

E-mail address: p.hicks@abdn.ac.uk

forcing. Figure 1 shows schematics of both flow domains and associated forcing. Currently the only work on laminar streak growth above an oscillating plate assumes a parallel boundary layer flow structure, while the disturbance growth is excited by the continuous spectrum of the Orr-Sommerfeld equation¹⁶. A recent study has shown that this use of the continuous spectrum of the Orr-Sommerfeld equation is inappropriate to describe the penetration of free-stream turbulence into a laminar boundary layer¹⁷.

In an incompressible flow of density ρ^* , which is non-dimensionalized by the far-field velocity U_∞^* , the spanwise wavelength of the free-stream disturbance λ_z^* , and pressures $\rho^* U_\infty^{*2}$; a vortical free-stream disturbance of the form

$$\mathbf{u} = \hat{\mathbf{i}} + \varepsilon \hat{\mathbf{u}}^\infty e^{i(k_x x + k_y y + k_z z - k_x t)} + c.c., \tag{1}$$

is assumed, where ε is a measure of the turbulence intensity of the free stream and *c.c.* indicates the complex conjugate. The components of the free-stream disturbance velocity $\hat{\mathbf{u}}^\infty = (\hat{u}^\infty, \hat{v}^\infty, \hat{w}^\infty)$ and the wave numbers $\mathbf{k} = (k_x, k_y, k_z)$, satisfy the solenoidal condition $\hat{\mathbf{u}}^\infty \cdot \mathbf{k} = 0$. If the dynamic viscosity of the fluid is μ^* , then a Reynolds number $R_\lambda = \rho^* U_\infty^* \lambda_z^* / \mu^*$ can be formed, which in the regime of interest is expected to be much greater than one. The flow structure is linearised by the small value of the turbulent Reynolds number εR_λ , while, to retain the spanwise momentum diffusion necessary for streak interactions, we must consider distances $\bar{x} \sim x/R_\lambda$ downstream from the leading edge.

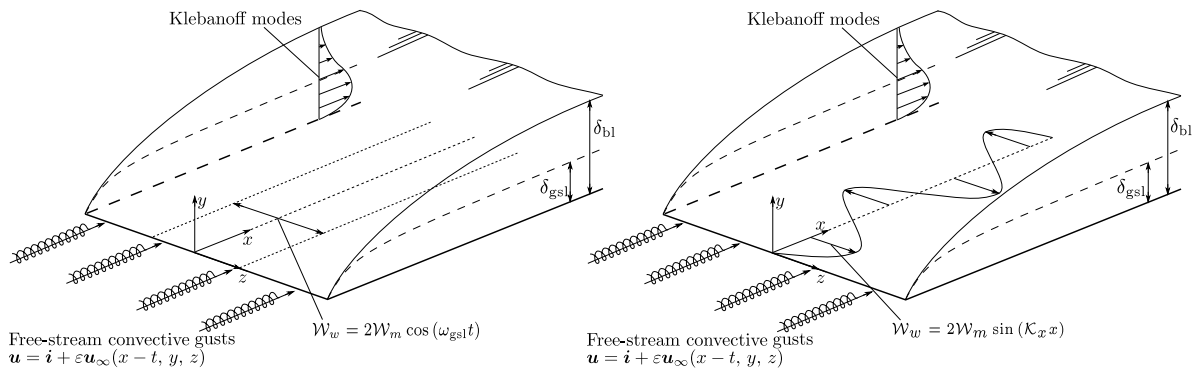


Fig. 1: An illustration of free-stream convective gusts interacting with a spanwise oscillating plate (left) and a plate with steady spanwise sinusoidal forcing (right).

Experimental results have shown that free-stream vortical disturbances with $k_x \ll k_y$, $k_x \ll k_z$ and $k_y/k_z = O(1)$ penetrate most deeply into the boundary layer¹. In the distinguished limit $R_\lambda \gg 1$ and $k_x R_\lambda = O(1)$, a coupled system of equations is found linking the spanwise base flow and the disturbance flow in the Linearized Unsteady Boundary Region (LUBR) of Leib *et al.*³. In §2 the base flows are described, while §3 outlines the LUBR equation structure. Comparative results and energy reductions produced by both spanwise forcing types are described in §4, before conclusions are drawn in §5.

2. Base flow behaviour

For both forcing types the streamwise and wall-normal base flows match the Blasius boundary layer. On the flat plate $y = 0$ and $\bar{x} > 0$, the spanwise base flow satisfies the boundary condition $W_{\text{oscil}} = 2W_m \cos(\bar{\omega} \bar{t})$ in the case of spanwise plate oscillations and $W_{\text{force}} = 2W_m \sin(\mathcal{K}_x \bar{x})$ in the case of steady spanwise forcing. Here $2W_m$ is the amplitude of the oscillation, the Strouhal number $\bar{\omega}$ is the ratio of the plate oscillation frequency to the convective time scale of the gust, and \mathcal{K}_x is the ratio of the streamwise gust wavelength to the wavelength of the forcing. The scaled spanwise base flow above an oscillating plate, W_{oscil} , is time periodic and therefore can be decomposed as

$$W_{\text{oscil}}(\bar{x}, \eta, \bar{t}) = W(\bar{x}, \eta) e^{i\bar{\omega} \bar{t}} + W^*(\bar{x}, \eta) e^{-i\bar{\omega} \bar{t}}, \tag{2}$$

where $*$ denotes a complex conjugate, $\bar{t} = k_x t$, $\bar{x} = k_x x$ and the wall-normal Blasius similarity variable $\eta = y(R_\lambda/2x)^{1/2}$. The streamwise and wall-normal dependence of the complex-valued W is determined by the parabolic

equation

$$i\bar{\omega}W + F' \frac{\partial W}{\partial \bar{x}} - \frac{F}{2\bar{x}} \frac{\partial W}{\partial \eta} = \frac{1}{2\bar{x}} \frac{\partial^2 W}{\partial \eta^2}, \quad (3)$$

subject to $W(\bar{x}, 0) = W_m$, $W \rightarrow 0$ as $\eta \rightarrow \infty$, and $W = W_m(1 - F')$ for \bar{x} small. Here F satisfies the Blasius equation $F''' + FF'' = 0$. The solutions to this equation satisfy a generalized Stokes layer (GSL), which retains non-parallel flow effects and consequently evolves along the streamwise direction.

For the oscillating plate, if a new streamwise coordinate $\hat{x} = N\bar{x}$ is defined, then the WBKJ ansatz

$$W = \bar{W}(\hat{x}, \eta) e^{-(2\hat{x})^{1/2} \Theta(\eta)}, \quad (4)$$

leads to

$$W_{\text{gsl}}|_{\hat{x} \gg 1} = \frac{W_m F''(\eta)}{F''(0)} \exp\left(\frac{F\eta}{2}\right) \exp[-\hat{x}^{1/2}(1+i)\eta] \exp(iN\bar{t}) + c.c. \quad (5)$$

Here large \hat{x} corresponds to either large downstream distances or at a fixed downstream distance a series of flows in which the plate oscillating frequency increases. It can be shown that the large- \hat{x} behaviour of the GSL tends to the classical Stokes layer (CSL) and in dimensional variables the profile is given by

$$W_{\text{gsl}}|_{\hat{x} \gg 1} \sim W_m \exp\left[-(1+i) \sqrt{\frac{\omega_{\text{gsl}}^*}{2\nu^*}} y^*\right] \exp(i\omega_{\text{gsl}}^* t^*) + c.c.. \quad (6)$$

This behaviour is verified in figure 2, which shows the convergence of the GSL and CSL at large downstream distances for $N = 1$ (top), and also at $\bar{x} = 0.5$ for increasing N (bottom). The right most column shows the similarity in the solutions for two different cases corresponding to $\hat{x} = 8$.

The dotted horizontal lines in figure 2 correspond to the Blasius boundary layer thickness $0.99U_\infty^*$. For small \hat{x} the CSL penetrates much further into the boundary layer than the GSL, which remains bounded within the Blasius boundary layer throughout. This is because the viscous effects in the spanwise momentum equation are now balanced by the steady convection term rather than the unsteady term. For increasing values of \hat{x} the proportion of the Blasius layer occupied by the GSL decreases.

For steady spanwise wall forcing the scaled spanwise base flow W_{force} satisfies the parabolic equation

$$F' \frac{\partial W_{\text{force}}}{\partial \bar{x}} - \frac{F}{2\bar{x}} \frac{\partial W_{\text{force}}}{\partial \eta} = \frac{1}{2\bar{x}} \frac{\partial^2 W_{\text{force}}}{\partial \eta^2}, \quad (7)$$

which matches (3) when $\bar{\omega} = 0$. Representative steady spanwise base flow velocity profiles with $\mathcal{K}_x = 5$ are shown in the top row of figure 2. The vertical extent of this spanwise base flow is roughly equivalent to that of the GSL base flow and also remains confined in the Blasius layer throughout.

3. Linearised Unsteady Boundary Region (LUBR) equations with spanwise forcing

The disturbance behaviour above a spanwise oscillating plate is expected to be periodic behaviour in z and \bar{t} , and hence the disturbance velocities and pressure are decomposed as Fourier series in these variables, while the scaled coefficient of the $[n]$ th mode depend upon \bar{x} and η . For integer values of the Strouhal number $\bar{\omega} = N$, this gives rise to

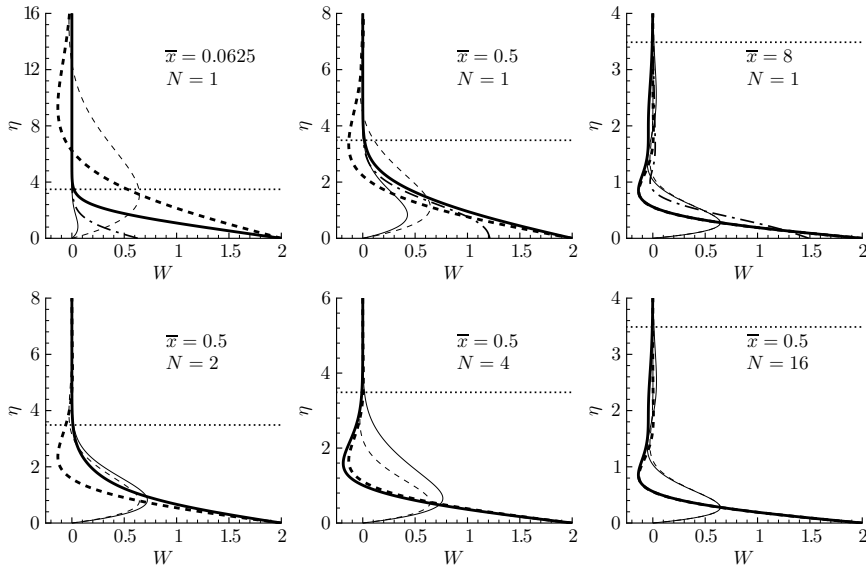


Fig. 2: Spanwise base flow profiles for the GSL (solid lines) and the CSL (dashed lines). The thick lines are $t = 0$ profiles while the thin lines are a $\pi/2$ phase shift. Also shown is a representative spanwise base flow with steady $\mathcal{K}_x = 5$ streamwise forcing (dot-dashed lines) and the Blasius boundary layer thickness $0.99U_\infty^*$ (dotted line).

equations governing linearised laminar streak growth in the form of a coupled system of modified LUBR equations:

$$\frac{\partial \bar{u}^{[n]}}{\partial \bar{x}} - \frac{\eta}{2\bar{x}} \frac{\partial \bar{u}^{[n]}}{\partial \eta} + \frac{\partial \bar{v}^{[n]}}{\partial \eta} + i\bar{w}^{[n]} = 0, \quad (8a)$$

$$\left(i n + \kappa_z^2 - \frac{\eta F''}{2\bar{x}} \right) \bar{u}^{[n]} + F' \frac{\partial \bar{u}^{[n]}}{\partial \bar{x}} - \frac{F}{2\bar{x}} \frac{\partial \bar{u}^{[n]}}{\partial \eta} - \frac{1}{2\bar{x}} \frac{\partial^2 \bar{u}^{[n]}}{\partial \eta^2} + F'' \bar{v}^{[n]} + iW \bar{u}^{[n-N]} + iW^* \bar{u}^{[n+N]} = 0, \quad (8b)$$

$$\left(i n + \kappa_z^2 + \frac{(\eta F')'}{2\bar{x}} \right) \bar{v}^{[n]} + F' \frac{\partial \bar{v}^{[n]}}{\partial \bar{x}} - \frac{F}{2\bar{x}} \frac{\partial \bar{v}^{[n]}}{\partial \eta} - \frac{1}{2\bar{x}} \frac{\partial^2 \bar{v}^{[n]}}{\partial \eta^2} + \frac{(F - \eta(\eta F')')}{(2\bar{x})^2} \bar{u}^{[n]} + \frac{1}{2\bar{x}} \frac{\partial \bar{p}^{[n]}}{\partial \eta} + iW \bar{v}^{[n-N]} + iW^* \bar{v}^{[n+N]} = 0, \quad (8c)$$

$$\begin{aligned} (i n + \kappa_z^2) \bar{w}^{[n]} + F' \frac{\partial \bar{w}^{[n]}}{\partial \bar{x}} - \frac{F}{2\bar{x}} \frac{\partial \bar{w}^{[n]}}{\partial \eta} - \frac{1}{2\bar{x}} \frac{\partial^2 \bar{w}^{[n]}}{\partial \eta^2} + i\kappa_z^2 \bar{p}^{[n]} + \left(\frac{\partial W}{\partial \bar{x}} - \frac{\eta}{2\bar{x}} \frac{\partial W}{\partial \eta} \right) \bar{u}^{[n-N]} + \frac{\partial W}{\partial \eta} \bar{v}^{[n-N]} \\ + iW \bar{w}^{[n-N]} + \left(\frac{\partial W^*}{\partial \bar{x}} - \frac{\eta}{2\bar{x}} \frac{\partial W^*}{\partial \eta} \right) \bar{u}^{[n+N]} + \frac{\partial W^*}{\partial \eta} \bar{v}^{[n+N]} + iW^* \bar{w}^{[n+N]} = 0, \end{aligned} \quad (8d)$$

where $\kappa_z = k_z / (k_x R_\lambda)^{1/2}$.

Similar equations have also been developed for the LUBR regime above a plate with spanwise wall forcing (see equations 8-11 of Ricco¹⁴). The key difference between the two sets of disturbance equations is that in the steady forcing case only a single mode (matching on to the free-stream gust) is forced while the remaining unforced modes are all zero. Above an oscillating plate, while only one mode is forced, the time dependent spanwise base flow couples unforced modes to the forced mode, leading to non-zero unforced modes. In the limit of negligible spanwise base flow, the LUBR equations for the oscillating plate case and for the steady spanwise wall forcing case simplify to give the LUBR equations of Leib *et al.*³ for streak growth above a stationary.

With both forms of spanwise forcing the initial and large- η boundary conditions for the LUBR equations associated with the forced mode essentially follow those derived by Leib *et al.*³ for flow above a stationary plate. These are derived by asymptotically matching the large- η limit of the LUBR equations to the free-stream gust behaviour at the edge of the boundary layer, and then producing initial conditions via a composite expansion involving a power series

for the small \bar{x} behaviour. The initial and large- η boundary conditions involve a scaled wall-normal wave-number $\kappa_y = k_y / (k_x R_\lambda)^{1/2}$, which for the cases shown is taken to equal κ_z . For the oscillating plate case only the $n = -1$ mode is forced, while the remaining modes in the Fourier series are zero initially (as the modes uncouple for \bar{x} small), and tend to zero in the far field.

4. Laminar streak profiles and energy reductions

For flow above an oscillating plate with $W_m = 8$, $N = 1$ and $\kappa_z = 1$, the streamwise velocity $\bar{u}_{\max}^{[n]}(\bar{x}) = \max_\eta \{ \bar{u}^{[n]}(\bar{x}, \eta) \}$, of the forced mode and the next six largest modes are shown in figure 3, alongside the corresponding wall-normal profiles of $\bar{u}^{[n]}$, $\bar{v}^{[n]}$ and $\bar{w}^{[n]}$ at $\bar{x} = 0.5$. The velocity associated with the forced mode initially increases rapidly compared to the unforced modes. The velocity of the unforced modes increase more slowly as a result of being coupled to the forced mode. The global maximum streamwise velocity associated with each mode moves downstream, while the maximum streamwise velocity over η moves closer to the wall as the index of a mode relative to the forced mode increases. The streak energy is dominated the streamwise velocity and hence the energy of the n th mode is obtained by integrating $|\bar{u}^{[n]}(\bar{x}, \eta)|^2$ over \bar{x} and η . The greatest energy is contained within the forced mode, while moving up and down the Fourier series away from this mode, the energy contained in each mode decays.

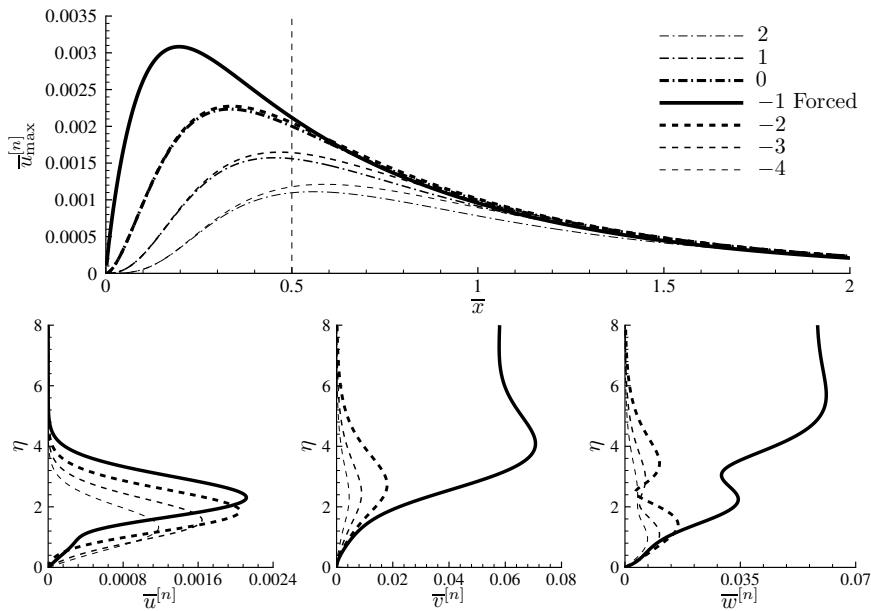


Fig. 3: The growth and decay of $\bar{u}_{\max}^{[n]}$ above an oscillating plate for $\kappa_z = 1$, $N = 1$ and $W_m = 8$ (top). The corresponding profiles of $\bar{u}^{[n]}$, $\bar{v}^{[n]}$ and $\bar{w}^{[n]}$ as functions of η at $\bar{x} = 0.5$ (bottom).

The streamwise root mean squared disturbance velocity,

$$\bar{u}_{\text{rms}}(\bar{x}, \eta) \equiv \left[2 \sum_{\substack{n=-\infty \\ n \neq 0}}^{\infty} |\bar{u}^{[n]}(\bar{x}, \eta)|^2 \right]^{1/2}, \tag{9}$$

while the total energy of the streak is calculated by integrating $|\bar{u}_{\text{rms}}(\bar{x}, \eta)|^2$ over both \bar{x} and η . The streamwise disturbance velocity maximum $\bar{u}_{\max}(\bar{x}) = \max_\eta \{ \bar{u}_{\text{rms}}(\bar{x}, \eta) \}$ is shown in figure 4 (left) for $N = 1$, $\kappa_z = 1$, and a range of different W_m . As W_m increases the global velocity maximum falls, with the maximum streamwise disturbance velocity

for $W_m = 16$ being nearly half the equivalent velocity above a stationary plate. The location of the velocity maxima moves upstream as W_m increases. Figure 4 (right) shows the corresponding reductions in relative streak energy

$$E_R = 100\% \left(\frac{E_{\text{stat}} - E_{\text{oscil}}}{E_{\text{stat}}} \right),$$

over a wider range of W_m values. For these free-stream-gust and plate-oscillation parameters a reduction in streak energy of over 80% is possible as the oscillation amplitude increases. However, for alternative parameters energy increases are also possible.

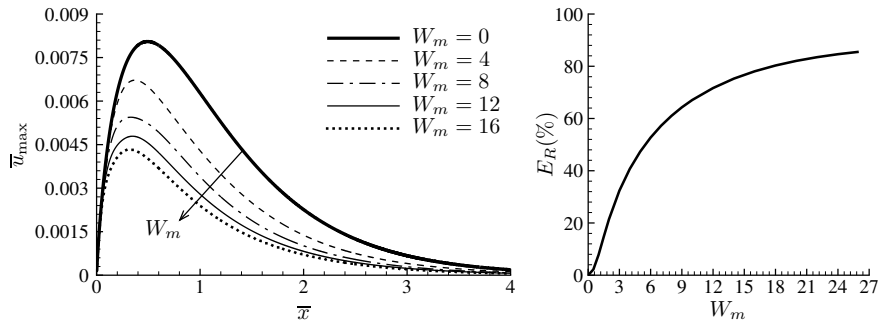


Fig. 4: Streamwise velocity evolution above an oscillating plate with changes in plate oscillation amplitude (left) and the percentage energy reduction with changes in plate oscillation amplitude (right), for $N = 1$ and $\kappa_z = 1$.

Variations in $\bar{u}_{\text{max}}(\bar{x})$ with increasing frequency ratios N are shown in figure 5 (left) for $W_m = 8$ and $\kappa_z = 1$. Compared to a streak above a stationary plate, lower streamwise velocities and streak energies are achieved in all the cases shown. Compared to the $N = 1$ streak, the streamwise disturbance velocities are higher in the tail of the streak when $N > 1$, with these differences propagating upstream towards the global velocity maximum as N increases. After rescaling time, profiles for $N < 1$ can be calculated. Representative samples of these cases are shown in figure 5 (right). These profiles correspond to cases in which the plate oscillations take longer than the free-stream gust oscillations. In these cases higher global streamwise disturbance velocity maxima are obtained as N decreases, which suggests that for $W_m = 8$ and $\kappa_z = 1$, the streak energy is minimized when $N = 1$.

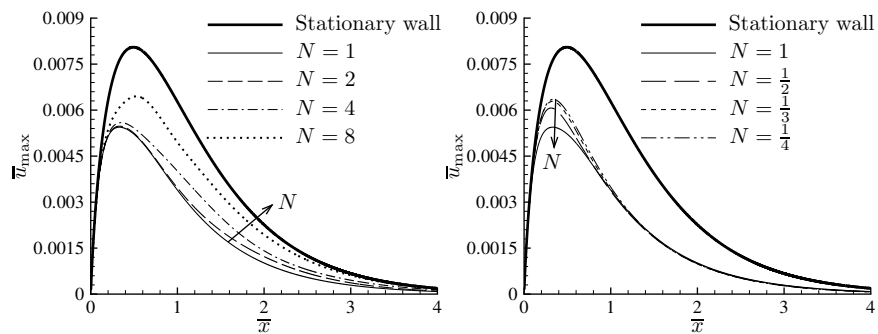


Fig. 5: Streamwise disturbance velocity evolution above an oscillating plate with $W_m = 8$ and $\kappa_z = 1$, for a range of frequency ratios N .

This result is confirmed and shown across a wider range of free-stream gust properties in figure 6. Over this range of κ_z , the value of N associated with the streak minimum energy increases with κ_z , with the minimum energy of $\kappa_z = 3$ streaks occurring when $N = 2$. The relative energy reductions on figure 6 (right) show that compared to a stationary

plate, streak energy reductions of nearly 90% are achieved when $\kappa_z = 0.5$, while streak energy increases occur for $\kappa_z = 3$ and $N < \frac{1}{2}$.

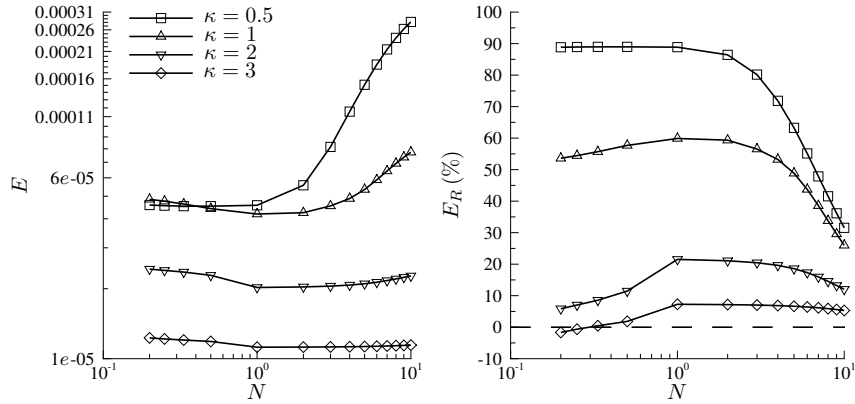


Fig. 6: Streak energy (left) and streak energy reduction relative to a stationary plate (right) for disturbances above an oscillating plate with $W_m = 8$, $\kappa_z = 1$ and a range of frequency ratios N .

4.1. Comparison with streaks generated with a classical Stokes layer

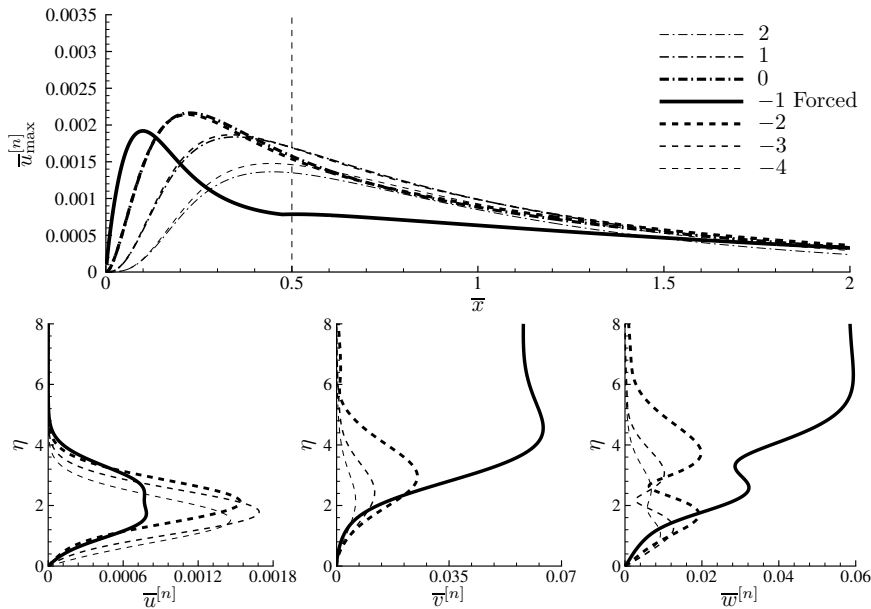


Fig. 7: As figure 3, but showing streaks forced by a CSL, rather than a GSL.

Figure 7 shows the same case as figure 3 except with a CSL spanwise base flow instead of a GSL. While for $\kappa_z = 1$, $W_m = 8$ and $N = 1$, the relative error in the streak energy induced by using a CSL rather than the GSL is less than 11%, there are significant differences between the underlying structure of the velocity modes. With the CSL the maximum

velocity associated with the forced mode is less than two-thirds of that of the GSL case. The maximum streamwise velocities with the CSL case are associated with unforced modes rather than the forced mode for $\bar{x} > 0.13$. This is because the CSL penetrates deeper into the boundary layer than the GSL for small \bar{x} (refer to figure 2), and hence more readily transfers energy away from the forced mode, producing higher velocities in the unforced modes.

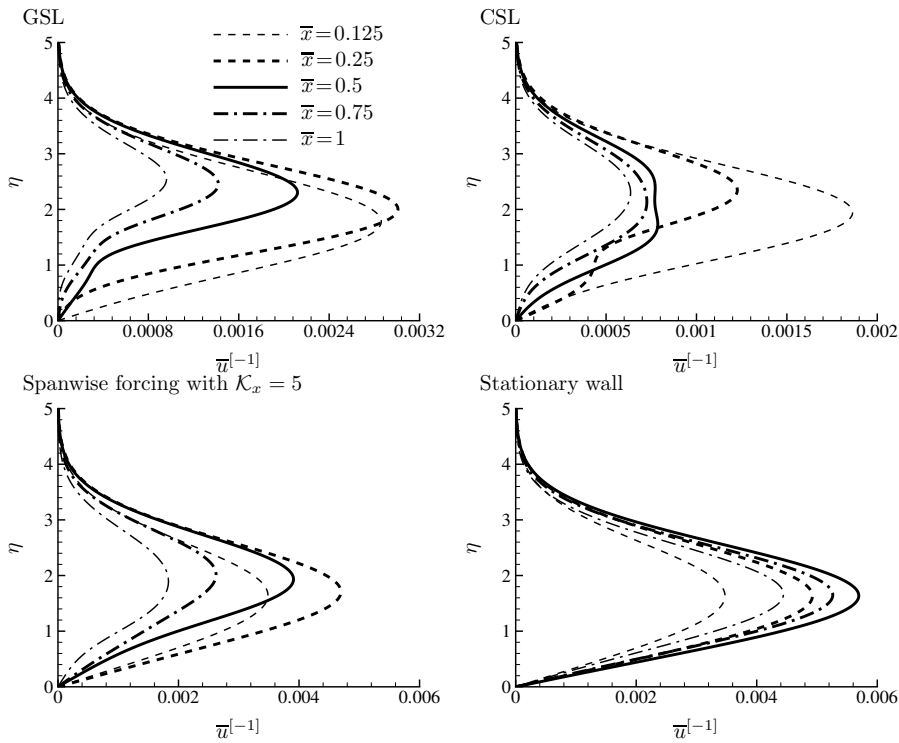


Fig. 8: A comparison of the streamwise disturbance velocity profiles of the forced mode for a GSL with $N = 1$ and $W_m = 8$ (top left), a CSL with $N = 1$ and $W_m = 8$ (top right), steady spanwise wall forcing with $\mathcal{K}_x = 5$ and $W_m = 9$ (bottom left) and a stationary wall (bottom right). In all cases $\kappa_z = 1$.

Wall-normal profiles of the streamwise disturbance velocity of the forced mode at a series of streamwise locations are shown in figure 8 for the GSL (top left), the CSL (top right) and a stationary plate (bottom right). The η height of the streamwise disturbance velocity maximum in a GSL increases with streamwise distance, while above a stationary plate these maxima have occur at a constant η . As a consequence of this, a reduction in the wall shear occurs with spanwise plate oscillations compared to a stationary plate. The corresponding profiles generated with the CSL contain multiple local velocity maxima, which are not observed in profiles created by the GSL or a stationary plate. The wall-normal position of these velocity maxima varies non-monotonically with increasing streamwise distance, and is neither fixed (like in a stationary plate), or moves away from the wall with streamwise distance (like in a GSL).

4.2. Comparison with streaks generated with steady spanwise wall forcing

Figure 9 shows the streak evolution and relative steak energy reductions for streaks above a plate with steady spanwise wall forcing with $\mathcal{K}_x = 5$. As with the oscillating plate case, reductions in streak velocity and energy are seen as W_m increases. Energy reductions for this particular wavelength ratio \mathcal{K}_x in excess of 90% are obtained. However, as with the oscillating plate, depending on the parameters associated with the free-stream gust and the forcing, smaller energy decreases and also significant energy increases are possible. More details of the streak behaviour with steady spanwise forcing can be found in Ricco¹⁴.

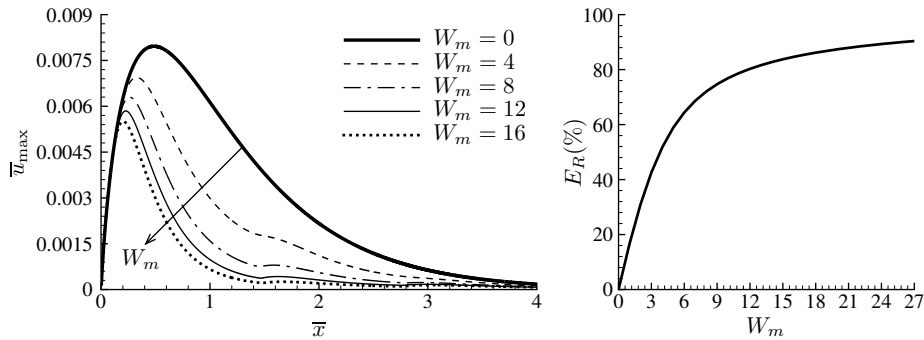


Fig. 9: As figure 4, except with steady sinusoidal spanwise wall forcing with $\mathcal{K}_x = 5$ rather than spanwise plate oscillations.

Wall-normal profiles for the forced mode streamwise disturbance velocity with steady spanwise forcing with $\mathcal{K}_x = 5$ are shown in figure 8 (bottom right). These exhibit many similarities with the profiles generated by spanwise plate oscillations, with both the η -height of the velocity maximum increasing with streamwise distance and reductions in wall shear compared to the stationary plate.

5. Conclusions

Equations governing laminar streak evolution in the linearized unsteady boundary region have been developed for flow above both a spanwise oscillating plate and a plate with steady sinusoidal spanwise wall forcing. These equations are natural generalizations of the LUBR equations of Leib *et al.*³ for flow above a stationary plate (which are recovered in the limit of vanishing spanwise base flow), and form an initial value problem with an explicit dependence on the free-stream vortical gust parameters. Both plate oscillations and steady spanwise wall forcing can produce streak energy reductions in excess of 80% across a range of different free-stream-gust and plate-motion parameters, although significant streak energy increases can also be obtained.

In the oscillating wall case it has been shown that the evolution of the spanwise base flow satisfies a GSL, which contains non-parallel flow effects and hence evolves with streamwise distance. A direct comparison with streaks forced by a CSL shows significant differences in the streak structure, indicating that it is inappropriate to force streaks above an oscillating plate with a CSL.

Spanwise plate oscillations and steady spanwise wall forcing are effective techniques for diminishing both the total streak energy of laminar streaks and their associated maximum disturbance velocity. While further experimental investigation is required to validate the effectiveness of these techniques, they can be added to boundary-layer suction and boundary-layer cooling as possible techniques for delaying laminar turbulent transition. Further results in the steady spanwise wall forcing case are contained in the paper by Ricco¹⁴, while a Journal of Fluid Mechanics paper currently under revision¹⁸ shows further results for the oscillating plate case.

Acknowledgements

This research was partially supported by EPSRC First Grant EP/I033173/1 and made use of computing resources at the University of Aberdeen and the University of Sheffield.

References

1. Matsubara, M., Alfredsson, P.H. Disturbance growth in boundary layers subjected to free-stream turbulence. *J Fluid Mech* 2001;**430**:149–168. doi:10.1017/S0022112000002810.
2. Mans, J., Kadijk, E.C., Lange, H.C.d., Steenhoven, A.A.v.. Breakdown in a boundary layer exposed to free-stream turbulence. *Exp Fluids* 2005;**39**(6):1071–1083. doi:10.1007/s00348-005-0040-6.

3. Leib, S.J., Wundrow, D.W., Goldstein, M.E.. Effect of free-stream turbulence and other vortical disturbances on a laminar boundary layer. *J Fluid Mech* 1999;**380**:169–203. doi:10.1017/S0022112098003504.
4. Ricco, P., Wu, X.. Response of a compressible laminar boundary layer to free-stream vortical disturbances. *J Fluid Mech* 2007;**587**:97–138. doi:10.1017/S0022112007007070.
5. Ricco, P.. The pre-transitional Klebanoff modes and other boundary-layer disturbances induced by small-wavelength free-stream vorticity. *J Fluid Mech* 2009;**638**:267–303. doi:10.1017/S0022112009990838.
6. Ricco, P., Luo, J., Wu, X.. Evolution and instability of unsteady nonlinear streaks generated by free-stream vortical disturbances. *J Fluid Mech* 2011;**677**:1–38. doi:10.1017/jfm.2011.41.
7. Byström, M.G., Levin, O., Henningson, D.S.. Optimal disturbances in suction boundary layers. *Eur J Mech B Fluids* 2007;**26**(3):330–343. doi:10.1016/j.euromechflu.2006.07.003.
8. Davidsson, E.N., Gustavsson, L.H.. Elementary solutions for streaky structures in boundary layers with and without suction. *Fluid Dyn Res* 2008;**40**(3):212–231. doi:10.1016/j.fluidyn.2007.08.002.
9. Ricco, P., Dilib, F.. The influence of wall suction and blowing on boundary-layer laminar streaks generated by free-stream vortical disturbances. *Phys Fluids* 2010;**22**(4):044101. doi:10.1063/1.3407651.
10. Ricco, P., Shah, D., Hicks, P.D.. Compressible laminar streaks with wall suction. *Phys Fluids* 2013;**25**(5):054110. doi:10.1063/1.4807066.
11. El-Hady, N.M.. Secondary instability of high-speed flows and the influence of wall cooling and suction. *Phys Fluids* 1992;**4**(4):727–743. doi:10.1063/1.858291.
12. Hubbard, S., Riley, N.. Boundary-layer control by heat and mass transfer. *Int J Heat Mass Trans* 1995;**38**(17):3209–3217. doi:10.1016/0017-9310(95)00070-P.
13. Ricco, P., Tran, D.L., Ye, G.. Wall heat transfer effects on Klebanoff modes and Tollmien–Schlichting waves in a compressible boundary layer. *Phys Fluids* 2009;**21**(2):024106. doi:10.1063/1.3054155.
14. Ricco, P.. Laminar streaks with spanwise wall forcing. *Phys Fluids* 2011;**23**(6):064103. doi:10.1063/1.3593469.
15. Galionis, I., Hall, P.. On the stabilization of the most amplified Görtler vortex on a concave surface by spanwise oscillations. *J Fluid Mech* 2005;**527**:265–283. doi:10.1017/S0022112004003118.
16. Hack, M.J.P., Zaki, T.A.. The continuous spectrum of time-harmonic shear layers. *Phys Fluids* 2012;**24**(3):034101. doi:10.1063/1.3687451.
17. Dong, M., Wu, X.. On continuous spectra of the Orr-Sommerfeld/Squire equations and entrainment of free-stream vortical disturbances. *J Fluid Mech* 2013;**732**:616–659. doi:10.1017/jfm.2013.421.
18. Hicks, P.D., Ricco, P.. Laminar streak growth above a spanwise oscillating wall. *Under revision for the J Fluid Mech* 2014;